

1 **Multiwavelength Observations of the Previously Unidentified**  
 2 **Blazar RX J0648.7+1516**

3 E. Aliu<sup>1</sup>, T. Aune<sup>2</sup>, M. Beilicke<sup>3</sup>, W. Benbow<sup>4</sup>, M. Böttcher<sup>5</sup>, A. Bouvier<sup>2</sup>,  
 4 S. M. Bradbury<sup>6</sup>, J. H. Buckley<sup>3</sup>, V. Bugaev<sup>3</sup>, A. Cannon<sup>7</sup>, A. Cesarini<sup>8</sup>, L. Ciupik<sup>9</sup>,  
 5 M. P. Connolly<sup>8</sup>, W. Cui<sup>10</sup>, G. Decerprit<sup>11</sup>, R. Dickherber<sup>3</sup>, C. Duke<sup>12</sup>, M. Errando<sup>1</sup>,  
 6 A. Falcone<sup>13</sup>, Q. Feng<sup>10</sup>, G. Finnegan<sup>14</sup>, L. Fortson<sup>15</sup>, A. Furniss<sup>2,\*</sup>, N. Galante<sup>4</sup>, D. Gall<sup>16</sup>,  
 7 G. H. Gillanders<sup>8</sup>, S. Godambe<sup>14</sup>, S. Griffin<sup>17</sup>, J. Grube<sup>9</sup>, G. Gyuk<sup>9</sup>, D. Hanna<sup>17</sup>,  
 8 B. Hivick<sup>5</sup>, J. Holder<sup>18</sup>, H. Huan<sup>19</sup>, G. Hughes<sup>11</sup>, C. M. Hui<sup>14</sup>, T. B. Humensky<sup>19</sup>,  
 9 P. Kaaret<sup>16</sup>, N. Karlsson<sup>15</sup>, M. Kertzman<sup>20</sup>, D. Kieda<sup>14</sup>, H. Krawczynski<sup>3</sup>, F. Krennrich<sup>21</sup>,  
 10 G. Maier<sup>11</sup>, P. Majumdar<sup>22</sup>, S. McArthur<sup>3</sup>, A. McCann<sup>17</sup>, P. Moriarty<sup>23</sup>, R. Mukherjee<sup>1</sup>,  
 11 T. Nelson<sup>30</sup>, R. A. Ong<sup>22</sup>, M. Orr<sup>21</sup>, A. N. Otte<sup>2</sup>, N. Park<sup>19</sup>, J. S. Perkins<sup>24,25</sup>, A. Pichel<sup>26</sup>,  
 12 M. Pohl<sup>27,11</sup>, H. Prokoph<sup>11</sup>, J. Quinn<sup>7</sup>, K. Ragan<sup>17</sup>, L. C. Reyes<sup>19</sup>, P. T. Reynolds<sup>28</sup>,  
 13 E. Roache<sup>4</sup>, H. J. Rose<sup>6</sup>, J. Ruppel<sup>27,11</sup>, D. B. Saxon<sup>18</sup>, G. H. Sembroski<sup>10</sup>, C. Skole<sup>11</sup>,  
 14 A. W. Smith<sup>29</sup>, D. Staszak<sup>17</sup>, G. Tešić<sup>17</sup>, M. Theiling<sup>4</sup>, S. Thibadeau<sup>3</sup>, K. Tsurusaki<sup>16</sup>,  
 15 J. Tyler<sup>17</sup>, A. Varlotta<sup>10</sup>, V. V. Vassiliev<sup>22</sup>, S. P. Wakely<sup>19</sup>, T. C. Weekes<sup>4</sup>, A. Weinstein<sup>21</sup>,  
 16 D. A. Williams<sup>2</sup>, B. Zitzer<sup>10</sup> (The VERITAS Collaboration)  
 17 S. Ciprini<sup>33</sup>, M. Fumagalli<sup>31,\*</sup>, K. Kaplan<sup>4</sup>, D. Paneque<sup>34,\*</sup>, J. X. Prochaska<sup>32</sup>

---

\*Corresponding authors: A. Furniss: afurniss@ucsc.edu, D. Paneque: dpaneque@mppmu.mpg.de, M. Fumagalli: miki@ucolick.org

<sup>1</sup>Department of Physics and Astronomy, Barnard College, Columbia University, NY 10027, USA

<sup>2</sup>Santa Cruz Institute for Particle Physics and Department of Physics, University of California, Santa Cruz, CA 95064, USA

<sup>3</sup>Department of Physics, Washington University, St. Louis, MO 63130, USA

<sup>4</sup>Fred Lawrence Whipple Observatory, Harvard-Smithsonian Center for Astrophysics, Amado, AZ 85645, USA

<sup>5</sup>Astrophysical Institute, Department of Physics and Astronomy, Ohio University, Athens, OH 45701, USA

<sup>6</sup>School of Physics and Astronomy, University of Leeds, Leeds, LS2 9JT, UK

<sup>7</sup>School of Physics, University College Dublin, Belfield, Dublin 4, Ireland

<sup>8</sup>School of Physics, National University of Ireland Galway, University Road, Galway, Ireland

<sup>9</sup>Astronomy Department, Adler Planetarium and Astronomy Museum, Chicago, IL 60605, USA

<sup>10</sup>Department of Physics, Purdue University, West Lafayette, IN 47907, USA

<sup>11</sup>DESY, Platanenallee 6, 15738 Zeuthen, Germany

<sup>12</sup>Department of Physics, Grinnell College, Grinnell, IA 50112-1690, USA

<sup>13</sup>Department of Astronomy and Astrophysics, 525 Davey Lab, Pennsylvania State University, University Park, PA 16802, USA

<sup>14</sup>Department of Physics and Astronomy, University of Utah, Salt Lake City, UT 84112, USA

<sup>15</sup>School of Physics and Astronomy, University of Minnesota, Minneapolis, MN 55455, USA

<sup>16</sup>Department of Physics and Astronomy, University of Iowa, Van Allen Hall, Iowa City, IA 52242, USA

<sup>17</sup>Physics Department, McGill University, Montreal, QC H3A 2T8, Canada

<sup>18</sup>Department of Physics and Astronomy and the Bartol Research Institute, University of Delaware, Newark, DE 19716, USA

<sup>19</sup>Enrico Fermi Institute, University of Chicago, Chicago, IL 60637, USA

<sup>20</sup>Department of Physics and Astronomy, DePauw University, Greencastle, IN 46135-0037, USA

<sup>21</sup>Department of Physics and Astronomy, Iowa State University, Ames, IA 50011, USA

<sup>22</sup>Department of Physics and Astronomy, University of California, Los Angeles, CA 90095, USA

<sup>23</sup>Department of Life and Physical Sciences, Galway-Mayo Institute of Technology, Dublin Road, Galway, Ireland

<sup>24</sup>CRESST and Astroparticle Physics Laboratory NASA/GSFC, Greenbelt, MD 20771, USA.

ABSTRACT

18

19

We report on the VERITAS discovery of very-high-energy (VHE) gamma-ray emission above 200 GeV from the high-frequency-peaked BL Lac object RX J0648.7+1516 (GB J0648+1516), associated with 1FGL J0648.8+1516. The photon spectrum above 200 GeV is fit by a power law  $dN/dE = F_0(E/E_0)^{-\Gamma}$  with a photon index  $\Gamma$  of  $4.4 \pm 0.8_{stat} \pm 0.3_{sys}$  and a flux normalization  $F_0$  of  $(2.3 \pm 0.5_{stat} \pm 1.2_{sys}) \times 10^{-11} \text{ TeV}^{-1}\text{cm}^{-2}\text{s}^{-1}$  with  $E_0 = 300 \text{ GeV}$ . No VHE variability is detected during VERITAS observations of RX J0648.7+1516 between 2010 March 4 and April 15. Following the VHE discovery, the optical identification and spectroscopic redshift were obtained using the Shane 3-m Telescope at the Lick Observatory, showing the unidentified object to be a BL Lac type with a redshift of  $z = 0.179$ . Broadband multiwavelength observations contemporaneous with the VERITAS exposure period can be used to sub-classify the blazar as a high-frequency-peaked BL Lac (HBL) object, including data from the MDM observatory, *Swift*-UVOT and XRT, and continuous monitoring at photon energies above 1 GeV from the *Fermi* Large Area Telescope (LAT). We find that in the absence of undetected, high-energy rapid variability, the one-zone synchrotron self-Compton model (SSC) overproduces the high-energy gamma-ray emission measured by the *Fermi*-LAT over 2.3 years. The SED can be parameterized satisfactorily with an external-Compton or lepto-hadronic model, which have two

---

<sup>25</sup>University of Maryland, Baltimore County, 1000 Hilltop Circle, Baltimore, MD 21250, USA.

<sup>26</sup>Instituto de Astronomia y Fisica del Espacio, Casilla de Correo 67 - Sucursal 28, (C1428ZAA) Ciudad Autnoma de Buenos Aires, Argentina

<sup>27</sup>Institut für Physik und Astronomie, Universität Potsdam, 14476 Potsdam-Golm, Germany

<sup>28</sup>Department of Applied Physics and Instrumentation, Cork Institute of Technology, Bishopstown, Cork, Ireland

<sup>29</sup>Argonne National Laboratory, 9700 S. Cass Avenue, Argonne, IL 60439, USA

<sup>30</sup>School of Physics and Astronomy, University of Minnesota, 116 Church St. SE, Minneapolis, MN 55455, USA

<sup>31</sup>Department of Astronomy and Astrophysics, University of California, 1156 High Street, Santa Cruz, CA 95064

<sup>32</sup>Department of Astronomy and Astrophysics, UCO/Lick Observatory, University of California, 1156 High Street, Santa Cruz, CA 95064

<sup>33</sup>Dipartimento di Fisica, Università degli Studi di Perugia, I-06123 Perugia, Italy

<sup>34</sup>Max-Planck-Institut für Physik, D-80805 München, Germany

and six additional free parameters, respectively, compared to the one-zone SSC model.

*Subject headings:* gamma rays: galaxies — BL Lacertae objects: individual  
(RX J0648.7+1516, 1FGL J0648.8+1516, VER J0648+152)

## 1. Introduction

1FGL J0648.8+1516 was detected by *Fermi*-LAT in the first 11 months of operation at greater than 10 standard deviations,  $\sigma$  (Abdo et al. 2010a). This source was flagged as a very-high-energy (VHE;  $E > 100$  GeV) emitting candidate by the *Fermi*-LAT collaboration by searching for  $\geq 30$  GeV photons. This information triggered the VERITAS observations reported here. 1FGL J0648.8+1516 is found to be associated with RX J0648.7+1516, which was first discovered by ROSAT (Brinkmann et al. 1997). A radio counterpart was identified in the NRAO Green Bank survey (Becker et al. 1991). Two subsequent attempts to identify an optical counterpart were unsuccessful (Motch et al. 1998; Haakonsen et al. 2009).

At  $6^\circ$  off the Galactic plane and without optical spectroscopy, the nature of this object remained unknown until optical spectroscopy was obtained in response to the VERITAS detection. These observations allow the active galactic nucleus (AGN) to be classified as a BL Lac, a type of AGN that has a jet co-aligned closely with the Earth’s line of sight and displays weak emission lines. These AGN are characterized by non-thermal, double-peaked broadband spectral energy distributions (SED). Based on the radio and X-ray flux, the BL Lac can further be classified as a high-frequency-peaked BL Lac (HBL) (Padovani & Giommi 1995), or if classified by the location of its low-energy peak, a high-synchrotron-peaked BL Lac (HSP) (Abdo et al. 2010b).

## 2. Observations and Analysis

### 2.1. VERITAS

VERITAS comprises four imaging atmospheric Cherenkov telescopes and is sensitive to gamma-rays between  $\sim 100$  GeV and  $\sim 30$  TeV (Weekes et al. 2002; Holder et al. 2006). The VERITAS observations of RX J0648.7+1516 were completed between 2010 March 4 and April 15 (MJD 55259-55301), resulting in 19.3 hours of quality-selected live time. These observations were taken at  $0.5^\circ$  offset in each of four directions to enable simultaneous background estimation using the reflected-region method (Fomin et al. 1994).

48 The VERITAS events are parameterized by the principal moments of the elliptical  
 49 shower images, allowing cosmic-ray background rejection through a set of selection criteria  
 50 (cuts) which have been optimized *a priori* on a simulated, soft-spectrum (photon index 4.0)  
 51 source with a VHE flux 6.6% of that observed from the Crab Nebula. The cuts discard  
 52 images with fewer than  $\sim 50$  photoelectrons. Events with at least two telescope images  
 53 remaining are then cosmic-ray discriminated based on the mean-scaled-width (MSW) and  
 54 the mean-scaled-length (MSL) parameters. Events with  $MSW < 1.1$ ,  $MSL < 1.4$ , a height of  
 55 maximum Cherenkov emission  $> 8$  km and an angular distance to the reconstructed source  
 56 position in the camera ( $\theta$ ) of less than 0.14 degrees are kept as gamma-ray candidate events.  
 57 The results are reproduced in two independent analysis packages (Cogan 2008; Daniel 2008).  
 58 After background rejection, 2711 events remain in the source region, with 16722 events  
 59 remaining in the background regions (larger by a factor of 6.89). The 283 excess events  
 60 result in a significance of  $5.2\sigma$ , calculated using Equation 17 from Li & Ma (1983).

61 A differential power law  $dN/dE = F_o(E/300 \text{ GeV})^{-\Gamma}$  is fit to the VERITAS data  
 62 from 200 to 650 GeV, shown in the top panel of Figure 1. The fit ( $\chi^2 = 0.90$  with 3  
 63 degrees of freedom (DOF), probability of 0.83) results in a flux normalization of  $F_o = (2.3 \pm$   
 64  $0.5_{stat} \pm 1.2_{syst}) \times 10^{-11}$  photons  $\text{cm}^{-2} \text{ s}^{-1} \text{ TeV}^{-1}$  and an index of  $\Gamma = 4.4 \pm 0.8_{stat} \pm 0.3_{syst}$ ,  
 65 corresponding to 3.3% of the Crab Nebula flux above 200 GeV.

66 The angular distribution of the excess events is consistent with a point source now  
 67 designated VER J0648+152, located at  $102.19^\circ \pm 0.11^\circ_{stat}$  RA and  $15.27^\circ \pm 0.12^\circ_{stat}$  Dec  
 68 (J2000). The systematic pointing uncertainty of VERITAS is less than  $25''$  ( $7 \times 10^{-3}$  degrees).  
 69 This position is consistent with the radio position of RX J0648.7+1516 (Becker et al. 1991).  
 70 A nightly-binned VHE light curve is fit with a constant and shows a  $\chi^2$  null hypothesis  
 71 probability of 0.39, showing no significant variability during the observation.

## 72 2.2. *Fermi*-LAT

73 The *Fermi*-LAT is a pair-conversion telescope sensitive to photons between 20 MeV  
 74 and several hundred GeV (Atwood et al. 2009; Abdo et al. 2009). The data used in this  
 75 paper encompass the time interval 2008 Aug 5 through 2010 Nov 17 (MJD 54683-55517),  
 76 and were analyzed with the LAT `ScienceTools` software package version `v9r15p6`, which  
 77 is available from the Fermi Science Support Center (FSSC). Only events from the “diffuse”  
 78 class with energy above 1 GeV within a  $5^\circ$  radius of RX J0648.7+1516 and with a zenith  
 79 angle  $< 105^\circ$  were used. The background was parameterized with the files `gll_iem_v02.fit` and

80 isotropic\_iem\_v02.txt <sup>1</sup>. The normalizations of the components were allowed to vary freely  
 81 during the spectral point fitting, which was performed with the unbinned likelihood method  
 82 and using the instrument response function P6\_V3\_DIFFUSE.

83 The spectral fits using energies above 1 GeV are less sensitive to possible contamination  
 84 from unaccounted (transient) neighboring sources, and hence have smaller systematic errors,  
 85 at the expense of slightly reducing the number of source photons. Additionally, there is no  
 86 significant signal from RX J0648.7+1516 below 1 GeV. The analysis of 2.3 years between  
 87 2008 Aug 5 and 2010 Nov 17 (MJD 54683–55517) of *Fermi*-LAT events with energy between  
 88 0.3–1 GeV (fixing the spectral index to 1.89) yields a test statistic (TS) of 9, corresponding  
 89 to  $\sim 3\sigma$  <sup>2</sup>. In addition to the background, the emission model includes two nearby sources  
 90 from the 1FGL catalog: the pulsars PSR J0659+1414 and PSR J0633+1746. The spectra  
 91 from the pulsars are parameterized with power-law functions with exponential cutoffs, and  
 92 the values are fixed to the values found from 18 months of data. The spectral fluxes are  
 93 determined using an unbinned maximum likelihood method. The flux systematic uncertainty  
 94 is estimated as 5% at 560 MeV and 20% at 10 GeV and above.<sup>3</sup>

95 The results from the *Fermi*-LAT spectral analysis are shown in the bottom panel of  
 96 Figure 1. There is no variability detected in four time bins evenly spread over the 2.3  
 97 years of data. The dataset corresponding in time to the VERITAS observations between  
 98 between 2010 March 4 and April 15 (i.e. MJD 55259–55301) does not show any significant  
 99 signal and thus we report  $2\sigma$  upper limits that were computed using the Bayesian method  
 100 (Helene 1983), where the likelihood is integrated from zero up to the flux that encompasses  
 101 95% of the posterior probability. When using the data accumulated over the expanded full  
 102 2.3 years of data, we find that 1FGL J0648.8+1516 is significantly detected above 1 GeV  
 103 with a TS of 307. The spectrum is fit using a single power-law function with photon flux  
 104  $F_{>1\text{ GeV}} = (1.8 \pm 0.2_{stat}) \times 10^{-9}$  photons  $\text{cm}^{-2}\text{s}^{-1}$  and hard differential photon spectral index  
 105  $\Gamma_{LAT} = 1.89 \pm 0.10_{stat}$ . The analysis is also performed on five energy ranges equally spaced  
 106 on a log scale with the photon index fixed to 1.89 and only fitting the normalization. The  
 107 source is detected significantly (TS>25) in each energy bin except for the highest energy  
 108 (100-300 GeV), for which a 95% confidence level upper limit is calculated.

---

<sup>1</sup>The files are available at <http://fermi.gsfc.nasa.gov/ssc/data/access/lat/BackgroundModels.html>

<sup>2</sup>See Mattox et al. (1996) for TS definition.

<sup>3</sup>See [http://fermi.gsfc.nasa.gov/ssc/data/analysis/LAT\\_caveats.html](http://fermi.gsfc.nasa.gov/ssc/data/analysis/LAT_caveats.html)

### 2.3. *Swift*-XRT

109

110 The *Swift*-XRT (Gehrels et al. 2004; Burrows et al. 2005) data are analyzed with HEA-  
 111 SOFT6.9 and XSPEC version 12.6.0. Observations were taken in photon counting mode  
 112 with an average count rate of  $\sim 0.3$  counts per second and did not suffer from pile-up. Six  
 113 target-of-opportunity observations summing to 10.5 ks were collected on six different days  
 114 between 2010 March 18 and April 18 (MJD 55273 and 55304), inclusive. These observations  
 115 were combined with a response file created from summing each observation’s exposure file  
 116 using *ximage*. The photons are grouped by energy to require a minimum of 30 counts per  
 117 bin, and fit with an absorbed power law between 0.3 and 10 keV, allowing the neutral hy-  
 118 drogen (HI) column density to vary. A HI column density of  $1.94 \pm 0.14 \times 10^{21} \text{cm}^{-2}$  is found,  
 119 only slightly higher than the  $1.56 \times 10^{21} \text{cm}^{-2}$  quoted in Kalberla et al. (2005). The com-  
 120 bined X-ray energy spectrum is extracted with a fit ( $\chi^2 = 114$  for 88 DOF, null hypothesis  
 121 probability of  $3.2 \times 10^{-2}$ ) with a photon index of  $2.51 \pm 0.06$  and an integral flux between 0.3  
 122 and 10 keV of  $(1.24 \pm 0.03_{\text{stat}}) \times 10^{-11} \text{ ergs cm}^{-2} \text{ s}^{-1}$ . This corresponds to a 0.3 to 10 keV  
 123 rest frame luminosity of  $1.1 \times 10^{45} \text{ ergs s}^{-1}$ . The deabsorbed spectrum is used to constrain  
 124 modeling.

### 2.4. *Swift*-UVOT

125

126 The *Swift*-XRT observations were supplemented with UVOT exposures taken in the U,  
 127 UVM2, and UVW2 bands (centered at  $8.56 \times 10^{14} \text{ Hz}$ ,  $1.34 \times 10^{15} \text{ Hz}$ , and  $1.48 \times 10^{15} \text{ Hz}$ ,  
 128 respectively; Poole et al. (2008)). The UVOT photometry is performed using the HEASOFT  
 129 program *wvotsource*. The circular source region has a  $5''$  radius and the background regions  
 130 consist of several circles with radii between  $10 - 15''$  of nearby empty sky. The results are  
 131 reddening corrected using  $R(V)=3.32$  and  $E(B-V)=0.14$  (Schlegel et al. 1998). The Galactic  
 132 extinction coefficients were applied according to Fitzpatrick (1999), with the largest source  
 133 of error resulting from dereddening. A summary of the UVOT analysis results is given in  
 134 Table 1.

### 2.5. Optical MDM

135

136 The region around RX J0648.7+1516 was observed in the optical B, V, and R bands  
 137 with the 1.3-m McGraw-Hill Telescope of the MDM Observatory on four nights during 2010  
 138 April 1–5 (MJD 55287-55291). Exposure times ranged from 90 sec (R-band) to 120 sec  
 139 (B-band). Each night, five sequences of exposures in B, V, and R were taken. The raw data

140 were bias subtracted and flat-field corrected using standard routines in IRAF<sup>4</sup>. Aperture  
141 photometry is performed using the IRAF package DAOPHOT on the object as well as five  
142 comparison stars in the same field of view. Calibrated magnitudes of the comparison stars  
143 are taken from the NOMAD catalog<sup>5</sup>, and the magnitudes of the object are determined using  
144 comparative photometry methods. For the construction of the SED points, the magnitudes  
145 are extinction corrected based on the Schlegel et al. (1998) dust map with values taken  
146 from NASA Extragalactic Database (NED)<sup>6</sup> :  $A_B = 0.618$ ,  $A_V = 0.475$ , and  $A_R = 0.383$ .  
147 These data (summarized in Table 1) are used to constrain the modeling shown in this work,  
148 although the same conclusions result with the UVOT points as model constraint.

### 149 3. Spectroscopic Redshift Measurements

150 Two spectra were obtained during the nights of UT 2010 March 18 and 2010 November 6  
151 (MJD 55245 and 55506, respectively) with the KAST double spectrograph on the Shane 3-m  
152 Telescope at UCO/Lick Observatory. During the first night, the instrument was configured  
153 with a 600/5000 grating and 1.5" long slit, covering 4300 – 7100 Å. A single 1800 second  
154 exposure was acquired. During the night of November 6, another 1800 second exposure was  
155 acquired with a 600/4310 grism, D55 dichroic, a 600/7500 grating and 2" long slit, covering  
156 the interval 3500 – 8200 Å. The data were reduced with the LowRedux pipeline<sup>7</sup> and flux  
157 calibrated using a spectro-photometric star. The flux calibration is uncertain due to non-  
158 photometric conditions. Inspection of the March spectrum reveals Ca H+K absorption lines  
159 at redshift  $z = 0.179$ . This redshift is confirmed in the second spectrum at higher signal-to-  
160 noise (S/N) (S/N  $\sim 20$  in the blue and S/N  $\sim 50$  in the red) where Ca H+K, G band, Mg I  
161  $\lambda\lambda 5168, 5174, 5184$  and Na I  $\lambda\lambda 5891, 5894, 5897$  absorption lines with equivalent width  
162  $< 5$  Å are detected (see Figure 2 and Table 2 for details). No Ca H+K break is observed.  
163 These spectral features provide evidence for an early-type nature of the blazar host galaxy  
164 and allow for BL Lac classification, following Marcha et al. (1996) and Healey et al. (2007).

---

<sup>4</sup><http://www.noao.edu/credit.html>

<sup>5</sup><http://www.nofs.navy.mil/nomad.html>

<sup>6</sup><http://nedwww.ipac.caltech.edu/>

<sup>7</sup><http://www.ucolick.org/~xavier/LowRedux/index.html>



#### 4. Broadband SED Modeling

165

166 The contemporaneous multiwavelength data are matched with archival radio data from  
 167 NED and are shown in Figure 3. Since the radio data are not contemporaneous they are  
 168 shown only for reference. The synchrotron peak appears at a frequency greater than  $10^{16}$  Hz,  
 169 representing the first subclassification of RX J0648.7+1516, specifically as an HBL. These  
 170 data are used to test steady-state leptonic and lepto-hadronic jet models for the broadband  
 171 blazar emission. The absorption of VHE gamma rays by the extragalactic background light  
 172 (EBL) is accounted for through application of the Gilmore et al. (2009) EBL model; the  
 173 model of Finke et al. (2010) provides comparable results.

174

175 Leptonic models for blazar emission attribute the higher-energy peak in the SED to  
 176 the inverse-Compton scattering of lower-energy photons off a population of non-thermal,  
 177 relativistic electrons. These same electrons are responsible for the lower-energy synchrotron  
 178 emission making up the first peak. The target photon field involved in the Compton upscat-  
 179 tering can either be the synchrotron photons themselves, as in synchrotron self-Compton  
 180 (SSC) models, or a photon field external to the jet in the case of external Compton (EC)  
 181 models.

181

182 We use the equilibrium SSC model of Böttcher & Chiang (2002), as described in Acciari et al.  
 183 (2009). In this model, the emission originates from a spherical blob of relativistic electrons  
 184 with radius  $R$ . This blob is moving down the jet with a Lorentz factor  $\Gamma$ , corresponding to  
 185 a jet speed of  $\beta_{\Gamma}c$ . The jet is oriented such that the angle with respect to the line of sight is  
 186  $\theta_{\text{obs}}$ , which results in a Doppler boosting with Doppler factor  $D = (\Gamma[1 - \beta_{\Gamma} \cos \theta_{\text{obs}}])^{-1}$ . In  
 187 order to minimize the number of free parameters, the modeling is completed with  $\theta_{\text{obs}} = 1/\Gamma$ ,  
 188 for which  $\Gamma = D$ .

188

189 Within the model, electrons are injected with a power-law distribution at a rate  $Q(\gamma) =$   
 190  $Q_0\gamma^{-q}$  between the low- and high-energy cut-offs,  $\gamma_{1,2}$ . The electron spectral index of  
 191  $q = 4.8$  required for the models applied in this work might be the result of acceleration  
 192 in an oblique shock. While standard shock acceleration in relativistic, parallel shocks is  
 193 known to produce a canonical spectral index of  $\sim 2.2$ , oblique magnetic-field configurations  
 194 reduce the acceleration efficiency and lead to much steeper spectral indices (Meli & Quenby  
 195 2003; Sironi & Spitkovsky 2011). The radiation mechanisms considered lead to equilibrium  
 196 between the particle injection, radiative cooling and particle escape. The particle escape is  
 197 characterized with an efficiency factor  $\eta$ , such that the escape timescale  $t_{\text{esc}} = \eta R/c$ , with  
 198  $\eta = 100$  for this work. This results in a particle distribution streaming along the jet with  
 199 a power  $L_e$ . Synchrotron emission results from the presence of a tangled magnetic field  $B$ ,  
 200 with a Poynting flux luminosity of  $L_B$ . The parameters  $L_e$  and  $L_B$  allow the calculation of  
 the equipartition parameter  $\epsilon_{Be} \equiv L_B/L_e$ .

201 The top panel in Figure 3 shows the SSC model for RX J0648.7+1516, with parameters  
 202 summarized in Table 3. The model is marginally in agreement with the data only through use  
 203 of parameters well below equipartition. The *Fermi*-LAT contemporaneous 95% confidence  
 204 level upper limits in the energy ranges 1-3 GeV and 3-10 GeV are just above and below the  
 205 one-zone SSC model predictions. Additionally, these SSC model predictions are above the  
 206 2.3 year *Fermi*-LAT spectrum by more than a factor of 2, although this spectrum is not  
 207 contemporaneous with the other data. Variation of the model parameters within physically  
 208 reasonable values does not provide better agreement between model and data. Generally,  
 209 HBLs are well characterized by one-zone SSC models and hence these observations might  
 210 suggest the existence of one or more additional emission mechanisms that contribute to the  
 211 higher-energy peak.

212 An external-Compton model is also used to describe the data. The EC model is a  
 213 leptonic one-zone jet model with two additional parameters beyond the SSC parameters,  
 214 the thermal blackbody temperature  $T_{EC}$  and radiation energy density  $u_{EC}$  of the external  
 215 photon field, which is assumed to be isotropic and stationary in the blazar rest frame. The  
 216 EC model provides a better representation of the SED, as can be seen in the middle panel  
 217 of Figure 3, with the parameters listed in Table 3.

218 A lepto-hadronic model is also applied to the data. Within this model, ultrarelativistic  
 219 protons are the main source of the high-energy emission through proton synchrotron radi-  
 220 ation and pion production. The resulting spectra of the pion decay products are evaluated  
 221 with the templates of Kelner & Aharonian (2008). Additionally, a semi-analytical descrip-  
 222 tion is used to account for electromagnetic cascades initiated by the internal  $\gamma\gamma$  absorption  
 223 of multi-TeV photons by both the  $\pi^0$  decay photons and the synchrotron emission of ultra-  
 224 relativistic leptons, as explained in Böttcher (2010). Similar to the particle populations in  
 225 the leptonic models described above, this lepto-hadronic model assumes a power-law distri-  
 226 bution of relativistic protons,  $n(\gamma) \propto \gamma^{-q}$  between a low- and high-energy cut-off,  $E_p^{\min, \max}$ .  
 227 This population of relativistic protons is propagating along the blazar jet and has a total  
 228 kinetic luminosity of  $L_p$ . The lepto-hadronic modeling results are above  $\epsilon_{Bp}$  equipartition  
 229 and are shown in the bottom panel of Figure 3 with parameters (including energy partition  
 230 fractions  $\epsilon_{Bp} \equiv L_B/L_p$  and  $\epsilon_{ep} \equiv L_e/L_p$ ) summarized in Table 3.

231 In conclusion, multiwavelength followup of the VERITAS detection of 1FGL J0648.7+1516  
 232 has solidified its association with RX J0648.7+1516, which is identified as a BL Lac object  
 233 of the HBL subclass. Other contemporaneous SEDs of VHE-detected HBLs can be well  
 234 described by one-zone SSC models close to equipartition, while for RX J0648.7+1516 this  
 235 model provides a poor representation with parameters below equipartition. The addition  
 236 of an external photon field for Compton up-scattering in the leptonic paradigm provides

237 a better representation of the gamma-ray (*Fermi* and VERITAS) data. Alternatively, a  
238 leptohadronic model is successful in characterizing the higher-energy peak of the SED with  
239 synchrotron emission from protons. Both of these latter models require super-equipartition  
240 conditions.

241 The authors of the paper thank the ApJ referee for the well organized and constructive  
242 comments that helped to improve the quality and clarity of this publication.

243 VERITAS is supported by the US Department of Energy, US National Science Foun-  
244 dation and Smithsonian Institution, by NSERC in Canada, by Science Foundation Ireland  
245 (SFI 10/RFP/AST2748), and STFC in the UK. We acknowledge the excellent work of the  
246 technical support staff at the FLWO and at the collaborating institutions. This work was  
247 also supported by NASA grants from the Swift (NNX10AF89G) and Fermi (NNX09AU18G)  
248 Guest Investigator programs.

249 The *Fermi* LAT Collaboration acknowledges generous support from a number of agen-  
250 cies and institutes that have supported the development and the operation of the LAT as well  
251 as scientific data analysis. These include the National Aeronautics and Space Administration  
252 and the Department of Energy in the United States, the Commissariat à l’Energie Atom-  
253 ique and the Centre National de la Recherche Scientifique / Institut National de Physique  
254 Nucléaire et de Physique des Particules in France, the Agenzia Spaziale Italiana and the  
255 Istituto Nazionale di Fisica Nucleare in Italy, the Ministry of Education, Culture, Sports,  
256 Science and Technology (MEXT), High Energy Accelerator Research Organization (KEK)  
257 and Japan Aerospace Exploration Agency (JAXA) in Japan, and the K. A. Wallenberg Foun-  
258 dation, the Swedish Research Council and the Swedish National Space Board in Sweden.

259 Additional support for science analysis during the operations phase is acknowledged from  
260 the Istituto Nazionale di Astrofisica in Italy and the Centre National d’Études Spatiales in  
261 France.

262 J.X.P. acknowledges funding through an NSF CAREER grant (AST-0548180).

263 *Facilities:* VERITAS, Fermi, Swift, Lick, MDM.

## 264 REFERENCES

265 Abdo, A. et al. 2009, *Astroparticle Physics*, 32, 193

266 Abdo, A. et al. 2010, *ApJS*, 188, 405

- 267 Abdo, A. et al. 2010, *ApJ*, 716, 30
- 268 Atwood, W. B., et al. 2009, *ApJ*, 697, 1071
- 269 Acciari, V. A. et al. 2009, *ApJ*, 707, 612
- 270 Becker, R. et al. 1991, *ApJS*, 75, 1
- 271 Brinkmann, W. et al. 1997 *A&A*, 323, 739
- 272 Böttcher, M., & Chiang, J., 2002, *ApJ*, 581, 127
- 273 Böttcher, M., 2010, in proc. of “Fermi Meets Jansky”, eds. T. Savolainen, E. Ros, R. W.  
274 Porcas, & J. A. Zensus; p. 41
- 275 Burrows, D.N., Hill, J.E., Nousek, J.A., et al. 2005, *Space Sci. Rev.*, 120, 165
- 276 Cogan, P. 2008, Proc. 30th Int. Cosmic Ray Conf., Vol 3, The VERITAS Gamma-ray Anal-  
277 ysis Suite, ed. R. Caballero, J. C. D’Olivo, G. Medina-Tanco, L. Nellen, F. A. Sánchez  
278 & J. F. Valdeé-Galicia (Mexico City, Mexico: Universidad Nacional Autónoma de  
279 México), 1385
- 280 Daniel, M. 2008, Proc. 30th Int. Cosmic Ray Conf., Vol 3, The VERITAS Standard Data  
281 Analysis, ed. R. Caballero, J. C. D’Olivo, G. Medina-Tanco, L. Nellen, F. A. Sánchez  
282 & J. F. Valdeé-Galicia (Mexico City, Mexico: Universidad Nacional Autónoma de  
283 México), 1325
- 284 Gilmore, R. et al. 2009, *MNRAS*, 399, 1694
- 285 Helene, O. 1983, *Nuclear Instruments & Methods in Physics Research*, 212, 319
- 286 Fitzpatrick, E. 1999, *PASP*, 111, 63
- 287 Finke, J. et al. 2010, *ApJ*, 712, 238
- 288 Fomin, V. P. et al. 1994, *Astropart. Phys.*, 2, 137
- 289 Gehrels, N. et al. 2004, *ApJ*, 611, 1005
- 290 Healey, S. et al. 2007, *ApJS*, 171, 61
- 291 Haakonsen, C. B. et al. 2009, *ApJS*, 184, 138
- 292 Holder, J. et al. 2006, *Astropart. Phys.*, 25, 391

- 293 Kalberla, P. et al. 2005, *A&A*, 440, 775
- 294 Kelner, S. R. & Aharonian, F. A., 2008, *Phys. Rev. D.*, 78, 3, 034013
- 295 Li, T. & Ma, Y. 1983, *ApJ*, 272, 317
- 296 Marcha, M. et al. 1996, *MNRAS*, 281, 425
- 297 Mattox, J. et al. 1996, *ApJ*, 461, 396
- 298 Meli, A., & Quenby, J., 2003, *ApJ*, 19, 649
- 299 Motch, C. et al. 1998, *A&AS*, 132, 341
- 300 Padovani, P. & Giommi, P., 1995, *ApJ*, 444, 567
- 301 Poole et al. 2008, *MNRAS*, 383, 627
- 302 Shlegel, D. et al. 1998, *ApJ*, 500, 525
- 303 Sironi, L., & Spitkovsky, A. 2011, *ApJ*, 726, 75
- 304 Weekes, T. C. et al. 2002, *Astropart. Phys.*, 17, 221

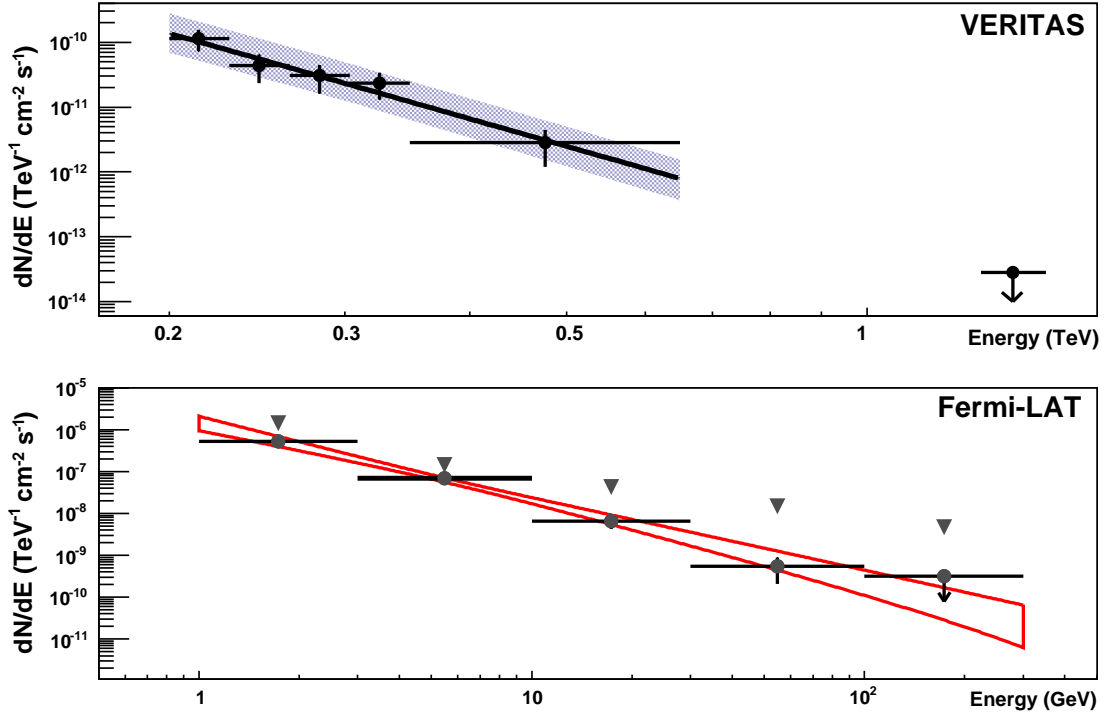


Fig. 1.— Top: The differential photon spectrum of RX J0648.7+1516 between 200 and 650 GeV measured by VERITAS between 2010 4 March and 15 April (MJD 55259–55301). The solid line shows a power-law fit to the measured flux derived with four equally log-spaced bins and a final bin boundary at 650 GeV, above which there are few on-source photons. A 99% confidence upper limit evaluated between 650 GeV and 5 TeV assuming a photon index of 4.4 is also shown. The shaded region shows the systematic uncertainty of the fit, which is dominated by 20% uncertainty on the energy scale. Bottom: The differential photon spectrum of RX J0648.7+1516 as measured by *Fermi*-LAT over 2.3 years between 2008 Aug 5 and 2010 Nov 17 (MJD 54683–55517, grey circles) with the highest energy bin containing a 95% confidence upper limit. *Fermi*-LAT upper limits from the VERITAS observation period are also shown (MJD 55259–55301, grey triangles).

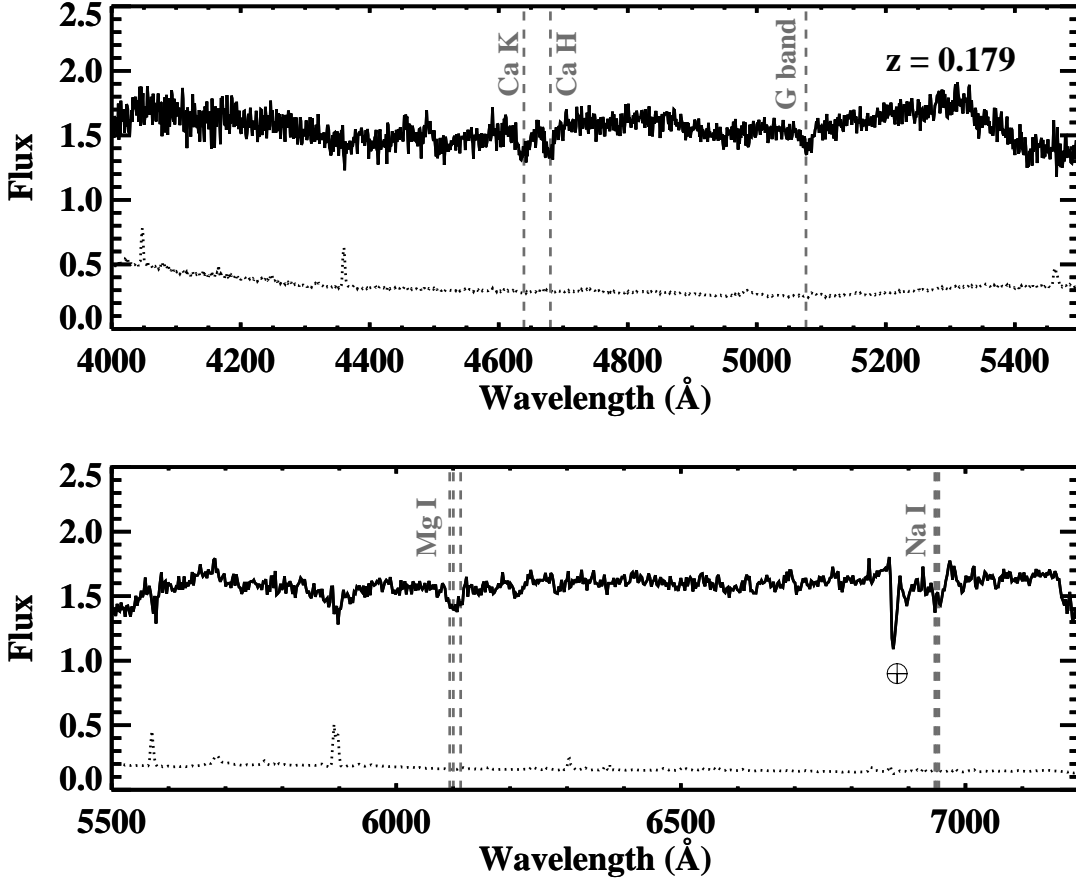


Fig. 2.— Spectrum of RX J0648.7+1516 showing the Ca H+K, G-band, NaI and MgI spectral features indicating a redshift of  $z = 0.179$ . Since the G-band arises in stellar atmospheres, we interpret this as the redshift for the host galaxy and not an intervening absorber. The blazar was observed at Lick Observatory using the 3–m Shane Telescope on 6 November 2010.

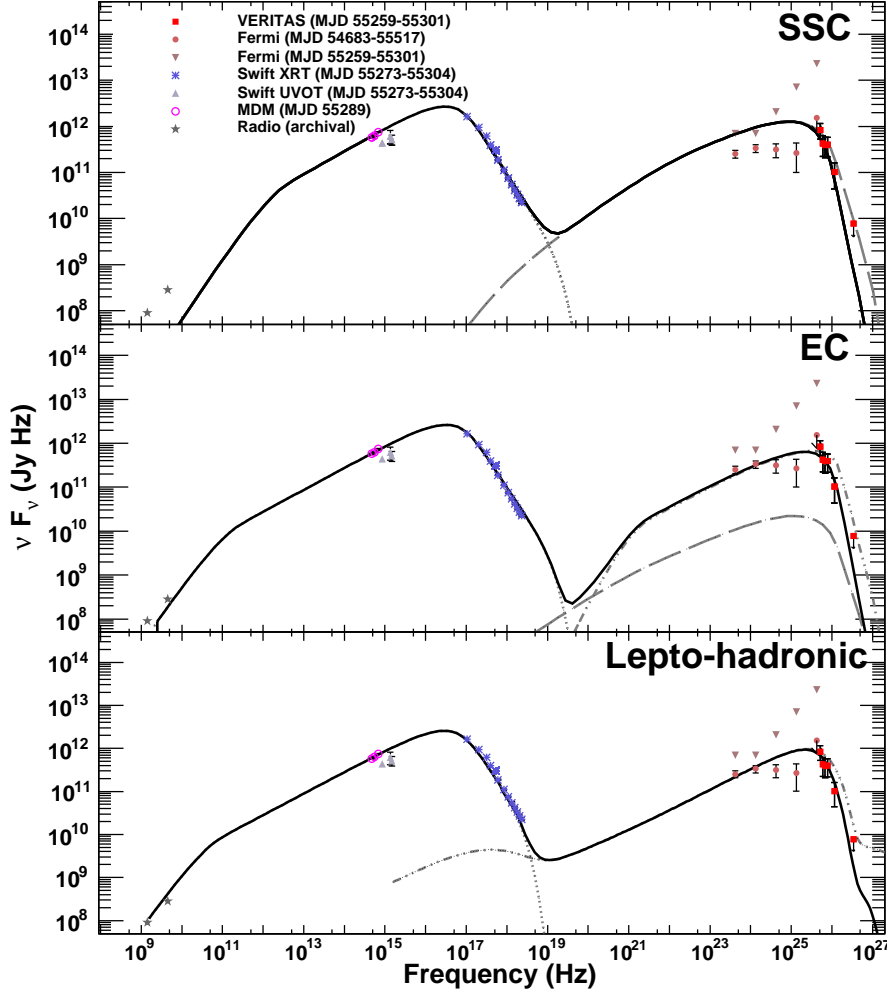


Fig. 3.— The SED models applied to the contemporaneous multiwavelength data of RX J0648.7+1516. *Fermi*-LAT data points are shown for 2.3 years of data along with upper limits extracted from data limited to the VERITAS observation period. The models shown here are constrained by the MDM points; modeling constrained by the UVOT data produces similar results. The top panel shows the synchrotron emission (dotted line), the self-Compton emission (dashed) and the EBL-corrected (Gilmore et al. 2009) total one-zone SSC model (solid). The middle panel shows the synchrotron emission (dotted line), the self-Compton emission (dashed line), the external-Compton (dash-dotted line) and the EBL-corrected total EC model (solid). The bottom panel shows the electron (and positron) synchrotron emission (dotted line), the proton synchrotron emission (dash-dotted) and the EBL-corrected total lepto-hadronic model (solid).



Table 1. Analysis summary of the optical MDM (B, V, R) and *Swift*-UVOT (U, UVM2, UVW2) data.

Band	Date (MJD)	$\nu F_\nu$ (Jy Hz)	$\nu F_\nu$ Error (Jy Hz)
B	55287	$7.47 \times 10^{11}$	$3.4 \times 10^{10}$
B	55289	$7.64 \times 10^{11}$	$3.8 \times 10^{10}$
B	55290	$5.75 \times 10^{11}$	$2.7 \times 10^{10}$
B	55291	$7.59 \times 10^{11}$	$3.4 \times 10^{10}$
V	55287	$5.77 \times 10^{11}$	$3.5 \times 10^{10}$
V	55289	$5.74 \times 10^{11}$	$3.7 \times 10^{10}$
V	55290	$2.92 \times 10^{11}$	$1.6 \times 10^{10}$
V	55291	$6.00 \times 10^{11}$	$3.6 \times 10^{10}$
R	55287	$5.99 \times 10^{11}$	$4.2 \times 10^{10}$
R	55289	$5.51 \times 10^{11}$	$3.7 \times 10^{10}$
R	55290	$2.03 \times 10^{11}$	$1.5 \times 10^{10}$
R	55291	$5.99 \times 10^{11}$	$4.3 \times 10^{10}$
U	55288	$4.542 \times 10^{11}$	$6.8 \times 10^9$
U	55292	$4.253 \times 10^{11}$	$6.3 \times 10^9$
U	55300	$3.856 \times 10^{11}$	$6.1 \times 10^9$
U	55304	$3.737 \times 10^{11}$	$5.5 \times 10^9$
UVM2	55274	$5.987 \times 10^{11}$	$8.8 \times 10^9$
UVW2	55273	$5.066 \times 10^{11}$	$7.9 \times 10^9$

Table 2. Analysis summary of the VER J0648+152 Lick Observatory Kast spectrum from 2010 November 5 (MJD 55505)

Ions	Rest Wavelength (Å)	Centroid <sup>a</sup> (Å)	FWHM (Å)	Redshift <sup>b</sup> Absorbed	Observed E. W. <sup>c</sup> (Å)	Notes
Ca II (K)	3934.79	4639.07	20.7	0.1789	$2.60 \pm 0.21$	
Ca II (H)	3969.61	4678.26	16.4	0.1785	$2.47 \pm 0.19$	
G band	4305.61	5077.46	17.5	0.1792	$1.70 \pm 0.18$	
Mg I	5174.14	6102.32	22.1	0.1793	$2.35 \pm 0.20$	[1]
Na I	5894.13	6951.66	23.0	0.1794	$2.48 \pm 0.15$	[2]

<sup>a</sup>Based on Gaussian fit

<sup>b</sup>Measured from line centroid

<sup>c</sup>Error is only statistical

Note. — [1] Blanded with Mg I 5168.74 Mg I 5185.04 [2] Blanded with Na I 5891.61 and Na I 5897.57

Table 3. SED Modeling Parameters: Summary of the parameters describing the emission-zone properties for the SSC, EC and lepto-hadronic models. See text for parameter descriptions.

Parameter	SSC	External Compton	Lepto-Hadronic
$L_e$ [erg s <sup>-1</sup> ]	$7.5 \times 10^{43}$	$4.9 \times 10^{41}$	$4.9 \times 10^{41}$
$\gamma_1$	$6.7 \times 10^4$	$8.2 \times 10^4$	$9 \times 10^3$
$\gamma_2$	$10^6$	$10^6$	$5 \times 10^4$
$q$	4.8	4.8	4.8
$B$ [G]	0.14	0.1	10
$\Gamma = D$	20	20	15
$T_{EC}$ [K]	—	$10^3$	—
$u_{EC}$ [erg cm <sup>-3</sup> ]	—	$7.0 \times 10^{-8}$	—
$L_p$ [erg s <sup>-1</sup> ]	—	—	$4.9 \times 10^{41}$
$E_p^{\min}$ [GeV]	—	—	$10^3$
$E_p^{\max}$ [GeV]	—	—	$1.5 \times 10^{10}$
$q_p$	—	—	2.0
$\epsilon_{Be}$	0.16	41	$1.7 \times 10^4$
$\epsilon_{Bp}$	—	—	4.2
$\epsilon_{ep}$	—	—	$2.5 \times 10^{-4}$
$t_{\text{var}}^{\min}$ [hr]	1.1	10.9	7.2